Gallium Switches the Selectivity of Classical Methanation Catalysts to Produce Methanol from CO_2

Wei Zhou[a‡], Colin Hansen[a‡], Weicheng Cao[a], Enzo Brack[a], Scott R. Docherty[a], Yuhao Wang[b], Chunliang Wang[b], Christian Ehinger[a], and Christophe Copéret[a*]

[a]*Department of Chemistry and Applied Biosciences, ETH Zürich, CH-8093 Zurich, Switzerland*

[b]*Engineering Research Center of Metallurgical Energy Conservation and Emission Reduction, Ministry of Education, Kunming University of Science and Technology, Kunming 650093, China*

‡These authors contributed equally to this work

*Corresponding author: ccoperet@inorg.chem.ethz.ch

Carbon dioxide is a major contributor to global climate change and ocean acidification, making efficient capture and utilization a required step for sustainable development. A pivotal aspect of sustainable development is to close the carbon cycle by converting CO_2 with "green" H_2 to value-added product or fuel, such as methanol[1-3]. In this context, supported metal catalysts have been extensively investigated, focusing on the role of promoters and/or supports to drive catalytic performance[4,5]. In particular, besides classical promoters like zinc[6,7], gallium has emerged as an alternative, to change properties from classical Cu-based methanol synthesis catalysts[8-10] to Ni-[11,12], Pd-[13-15] and Pt-based[16] systems. Here, we show that upon addition of Ga, the selectivity of group 8 and 9 transition-metal elements (Ru, Rh, Os and Ir), is switched from their widely-observed methanation behavior[17-19] to methanol synthesis catalysts, highlighting the universal propensity of Ga in promoting methanol formation. Detailed studies on the series of tailored silica-supported catalysts, amenable to *in situ* spectroscopy, complemented with density functional theory (DFT) calculations indicate that Ga is particularly prone to generate stable *M*Ga alloyed nanoparticles, that persist during CO_2 hydrogenation, driving methanol formation while suppressing the methanation reaction.

All catalysts – *M*Ga@SiO_2, *M* = Ru, Os, Rh, Ir – are prepared *via* Surface Organometallic Chemistry (SOMC) in order to enable a better control of the composition and the interface between the metal and the support[20,21]. Their synthesis involves grafting a molecular precursor on silica, already containing isolated surface OH groups and Ga^{III} surface sites (Ga^{III}@SiO_2, 0.8 Ga^{III} nm^{-2}), which itself is prepared by grafting of [Ga(OSi(O^{t}Bu)$_3$)$_3$(THF)] on silica partially dehydroxylated at 700 °C (SiO_2-

$_{700}$, 0.9 –OH nm^{-2}) and subsequent thermal treatment under high vacuum (10^{-5} mbar)[22]. Subsequent treatment under H_2 of the resulting bimetallic material generates silica-supported nanoparticles (Fig. 1a, Supplementary Fig. 1 and 2, see ESI for experimental details). For group 8 (Ru and Os), precursors of general structure M(*p*-cymene)(OSi(O^{t}Bu)$_3$)$_2$ (Supplementary Fig. 3-5) are selected[23], while for group 9 (Rh and Ir) metal precursors M(COD)(DIA), (COD = 1,5-*cis*,*cis*-cyclooctadiene, DIA = N,N'-diisopropylacetamidinate) (Supplementary Fig. 6-12) [24] are chosen because they can readily be grafted and then generate supported nanoparticles free of organic ligands upon treatment under a flow of H_2 at 400 °C, as evidenced by infrared (IR) spectroscopy (Fig. 1b, 1c, Supplementary Fig. 13, 14). The corresponding monometallic materials *M*@SiO_2 (*M* = Ru, Os, Rh, Ir) are also prepared through the same approach, using undoped $SiO_{2\text{-}700}$ in place of Ga^{III}@SiO_2 (Supplementary Fig. 15-18).

The metal loadings in bimetallic *M*Ga@SiO_2 materials and monometallic *M*@SiO_2 materials, as determined by inductively coupled plasma optical emission spectroscopy (ICP-OES), are comparable i.e. within a range of 0.50-0.85 *M*/nm^2 (metal density) and a *M*/Ga ratio close to 1 in *M*Ga@SiO_2 (Table S1). HAADF-STEM images show a narrow particle size distribution centered at 1.6-1.8 nm for all four bimetallic *M*Ga@SiO_2 materials (Fig. 1d-1g). In general, the nanoparticles are smaller than for the corresponding *M*@SiO_2, indicating a strong interaction between the transition metal *M* and the Ga promoter (Supplementary Fig. 21-23, Table S1). EDX images show that the Ga and *M* profiles overlap in all cases, suggesting the formation of *M*Ga alloys upon H_2 reduction (Supplementary Fig. 26-29). In fact, IR of the samples exposed to CO show a significant red-shift of the adsorbed CO on *M*Ga@SiO_2 vs. *M*@SiO_2 materials (Supplementary Fig. 30) [25,26], providing further evidence for alloying between *M* and Ga.

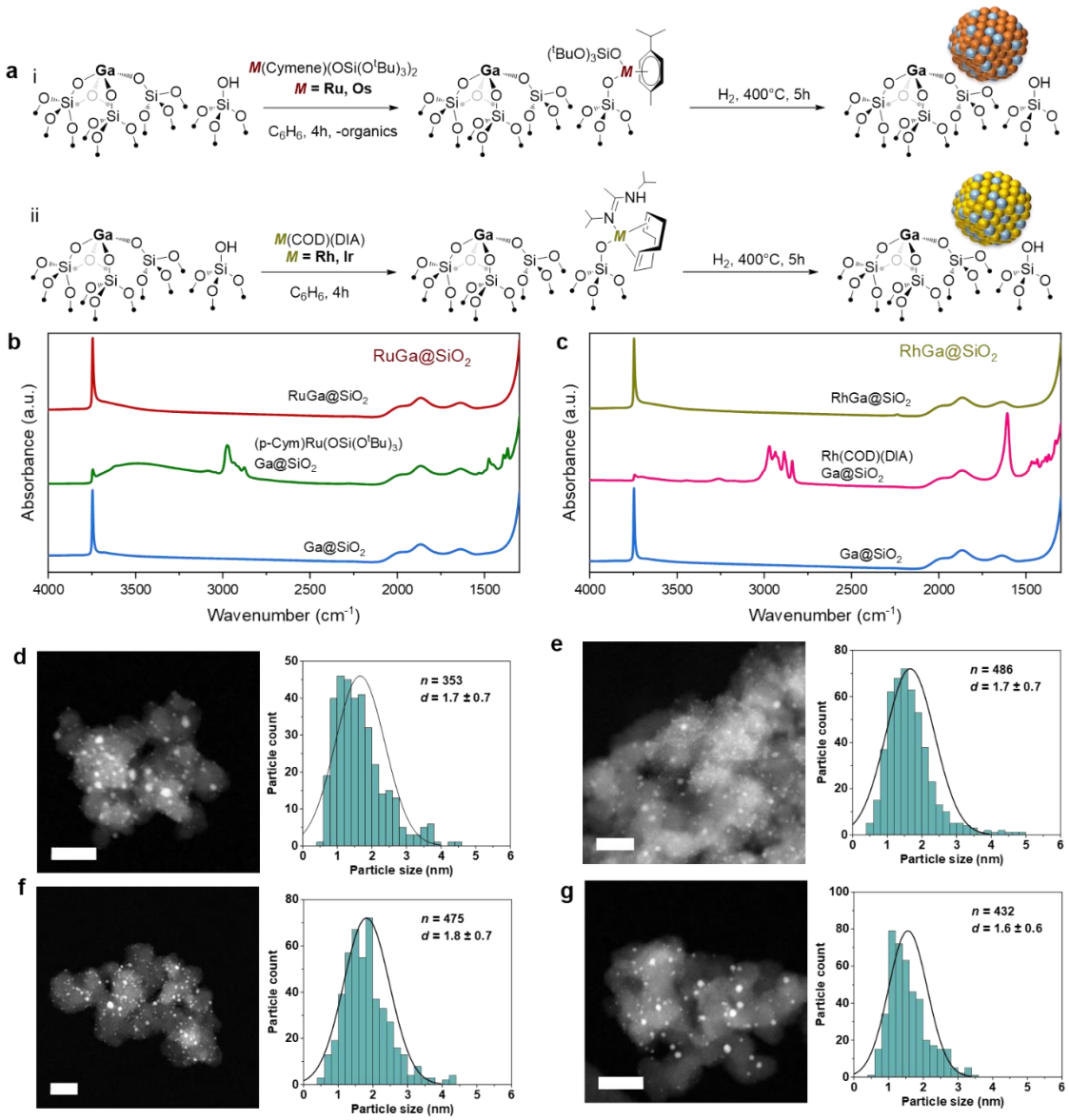

Fig. 1 | Preparation of *M*Ga@SiO$_2$ and *M*@SiO$_2$ materials. a, Schematic procedure for grafting of group 8 (Ru, Os) and group 9 (Rh, Ir) molecular precursors on Ga^{III}@SiO$_2$ followed by reduction under H_2 at 400 °C. IR spectra throughout the synthesis of RuGa@SiO$_2$ (**b**) and RhGa@SiO$_2$ (**c**) starting from the second grafting. High-angle annular dark-field STEM (HAADF-STEM) images and particle size distribution of RuGa@SiO$_2$ (**d**), RhGa@SiO$_2$ (**e**), OsGa@SiO$_2$ (**f**) and IrGa@SiO$_2$ (**g**). The scale bar measures 20 nm.

*M*Ga@SiO$_2$ and *M*@SiO$_2$ materials are next evaluated for CO_2 hydrogenation at 230 °C and 40 bar (H_2/CO_2/Ar = 3:1:1). Under these reaction conditions, methanol is the main product for most bimetallic catalysts, while monometallic systems produce essentially only methane and Ga@SiO$_2$ is inactive (below detection limit) (Supplementary Fig. 31-38). The intrinsic methanol formation rates over RuGa@SiO$_2$, OsGa@SiO$_2$, RhGa@SiO$_2$ and IrGa@SiO$_2$ are 2.0, 3.7, 2.0 and 2.1 mol h^{-1} mol_{TM}^{-1},

which compare well with other reported CO_2 hydrogenation catalysts, corresponding to the intrinsic methanol selectivities of 65%, 88%, 39% and 78% respectively (Fig. 2a, Table S2, S3). RhGa@SiO_2 displays a relatively lower methanol selectivity, which can be enhanced up to 50% upon tuning the Rh/Ga ratio (Supplementary Fig. 19, 20, 24, 25, 39-42, Table S2). In sharp contrast, the monometallic Rh@SiO_2, Ir@SiO_2, Ru@SiO_2 and Os@SiO_2 catalysts all show methane as the main product with high activity as expected for these metals (Fig. 2a, Table S2). Notably, the presence of Ga significantly suppresses the methanation activity, while promoting methanol formation. When comparing catalysts at 1% CO_2 conversion, the methane selectivity sharply decreases from > 97% for monometallic *M*@SiO_2 catalysts to below 20% for Ga-promoted systems, *M*Ga@SiO_2 (Fig. 2b, Table S4). All four *M*Ga@SiO_2 catalysts also produce CO and a small amount of dimethyl ether (DME), the latter likely due to the dehydration of CH_3OH over Lewis acidic sites of Ga,[10,15] bringing the overall selectivity towards CH_3OH/DME to 60%, 87%, 38% and 70% for RuGa@SiO_2, OsGa@SiO_2, RhGa@SiO_2 and IrGa@SiO_2, respectively.

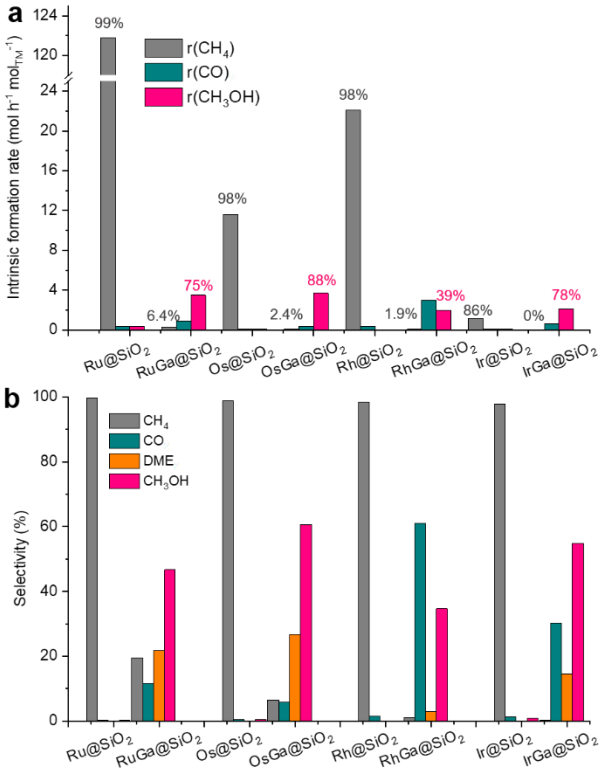

Fig. 2 | Catalytic performance of CO_2 hydrogenation over different catalysts. a, Intrinsic formation rates over monometallic *M*@SiO_2 and bimetallic *M*Ga@SiO_2 catalysts. **b,** Product selectivity over monometallic *M*@SiO_2 and bimetallic *M*Ga@SiO_2 catalysts at CO_2 conversion of 1%. Reaction conditions: F = 6-100 mL/min, T = 230

°C, P = 40 bar.

In order to understand the apparent universal promotional effect of Ga, the evolution of structure and chemical properties of all catalysts with the exception of Os-based systems is investigated under different conditions (exposed to air, reduced under H_2, post-CO_2 hydrogenation) by *in situ* X-ray Absorption Spectroscopy (XAS) experiments (Supplementary Fig. 43). The Ga-promoted bimetallic (MGa@SiO_2, M = Ru, Rh and Ir) catalysts are investigated at the M K-edge or L_3-edge and compared with the monometallic M@SiO_2. The corresponding best fits are shown in Supplementary Fig. 44-58 and summarized in Table S5-S7. First, the X-ray absorption near-energy structure (XANES) spectra of Ru K-edge and Rh K-edge for the air-exposed RuGa@SiO_2 and RhGa@SiO_2 catalysts display resemblances to metal oxide references, while the XANES Ir L_3-edge position and white line intensity for air-exposed IrGa@SiO_2 is similar to Ir foil. A similar difference is observed for the corresponding air-exposed monometallic M@SiO_2 catalysts: the XANES spectra for Ru is consistent with slightly oxidized metal (Supplementary Fig. 59-60), while Rh and Ir remain metallic (Supplementary Fig. 61-64). Regarding the extended X-ray absorption fine structure (EXAFS) of both air-exposed RuGa@SiO_2 and RhGa@SiO_2 catalysts, the fittings show a CN of 3.7 and 5.0 for Ru-O and Ru-Ru, and a CN of 2.2 and 4.0 for Rh-O and Rh-Rh, respectively (Fig. 3a-3d, Supplementary Fig. 47, 50, Table S5, S6), indicating a mixture of metallic and oxidized species, consistent with XANES. For IrGa@SiO_2 the EXAFS fitting shows a CN of 10.4 for the Ir-Ir scattering path, further supporting the presence of metallic Ir in air-exposed IrGa@SiO_2 as found in XANES (Fig. 3e, 3f, Supplementary Fig. 56, Table S7).

Next, the evolution of the air-exposed materials was monitored during H_2 temperature programed reduction (TPR) by XANES. With increasing temperatures, the white line intensities at the K-edges of both Ru and Rh gradually decrease and the edge position gradually shifts to lower energy, indicating the reduction of Ru and Rh in both RuGa@SiO_2 and RhGa@SiO_2 (Supplementary Fig. 65a, 65b). In fact, after H_2 reduction at 400 °C, the peaks belonging to metal oxides observed in the Fourier transform of the EXAFS spectra disappear, consistent with reduction. In addition, new peaks appear in the R-space between these expected for M-O and M-M (M = Ru or Rh) (Fig. 3b, 3d), and the EXAFS data for both systems are consistent with an average CN of 1.6 and 6.2 for Ru-Ga and Ru-Ru and an average CN of 3.6 and 2.3 for Rh-Ga and Rh-Rh, indicating alloying in both cases (Supplementary Fig. 48, 51, Table S5 and S6). For IrGa@SiO_2, the Ir L_3-edge XANES indicate a stepwise shift to higher energy

along with a decrease in the white line intensity during H_2 TPR (Supplementary Fig. 65c), indicative of a change of structure. After H_2 reduction, examination of the EXAFS shows that the peak at ca. 2.0 Å in R space become more intense compared to the second peak at ca. 2.5 Å, while this change is not observed in monometallic Ir@SiO_2 (Fig. 3f, Supplementary Fig. 64). These observations are consistent with the interaction between Ga and Ir, and EXAFS fitting reveals the presence of Ir-Ir scattering path ($CN_{Ir\text{-}Ir}$ = 9.2) as well as a low-degeneracy Ir-Ga path ($CN_{Ir\text{-}Ga}$ = 0.9) (Supplementary Fig. 57, Table S7) and thereby confirming IrGa alloy formation upon reduction. Note that, in the case of the monometallic *M*@SiO_2 materials, the XAS spectra are consistent with the exclusive presence of metallic nanoparticle after H_2 reduction at 400 °C (Supplementary Fig. 59-64, 66). After CO_2 hydrogenation, no change is observed for the XANES compared to the reduced materials. Similarly, the EXAFS spectra indicate similar CN for *M*-Ga in all three *M*Ga@SiO_2 systems, revealing that alloying remains throughout CO_2 hydrogenation (Fig. 3, Table S5-S7). Note that for the monometallic systems, *M* in *M*@SiO_2 all remains metallic, which is well-known for methanation catalysts (Supplementary Fig. 59-64, Table S5-S7).

In situ Ga K-edge XAS were also acquired under the same conditions in order to gain more insights into the interplay between *M* (*M* = Ru, Rh and Ir) and Ga in the *M*Ga@SiO_2 systems. In all cases, the XANES of Ga K-edge for the air-exposed *M*Ga@SiO_2 systems are similar to Ga^{III}@SiO_2 (Supplementary Fig. 67-69), while the edge position stepwise shifts to lower energy and the white line intensity decreases during H_2-TPR (Supplementary Fig. 70). These data suggest that the Ga^{III} is gradually reduced to Ga^0, which is probably incorporated into the nanoparticles to form *M*Ga alloyed nanoparticles during H_2 treatment as discussed above. A linear combination fitting (LCF) analysis of the spectra after H_2 reduction enables to evaluate the composition of *M*Ga nanoparticles (Supplementary Fig. 71, Table S8): the average ratios of *M*/Ga^0 are 3.0:1, 1.6:1 and 2.4:1 in RuGa, RhGa and IrGa alloyed nanoparticles respectively, indicating that the *M*Ga alloy contain ca. 25%-40% of Ga^0. Furthermore, all the Ga K-edge EXAFS can be fitted well using a model that includes Ga-O and Ga-*M* paths after H_2 reduction (Supplementary Fig. 72-80, Table S9). Overall, both the *M* K or L_3-edge and Ga K-edge spectroscopies demonstrate the formation of *M*-Ga alloy after H_2 reduction. Similar to what is found at the metal *M* edge, no change is observed at the Ga K-edge under CO_2 hydrogenation (Table S9), consistent with the stability of the alloy under these conditions. Overall, the XAS study at both *M* and Ga edges show that alloying between the metal and Ga is favored under H_2 and that the alloys remain stable under CO_2 hydrogenation conditions, paralleling the observed reactivity switch with the

selectivity changing from methane over pure metal *M* to methanol over *M*Ga alloy.

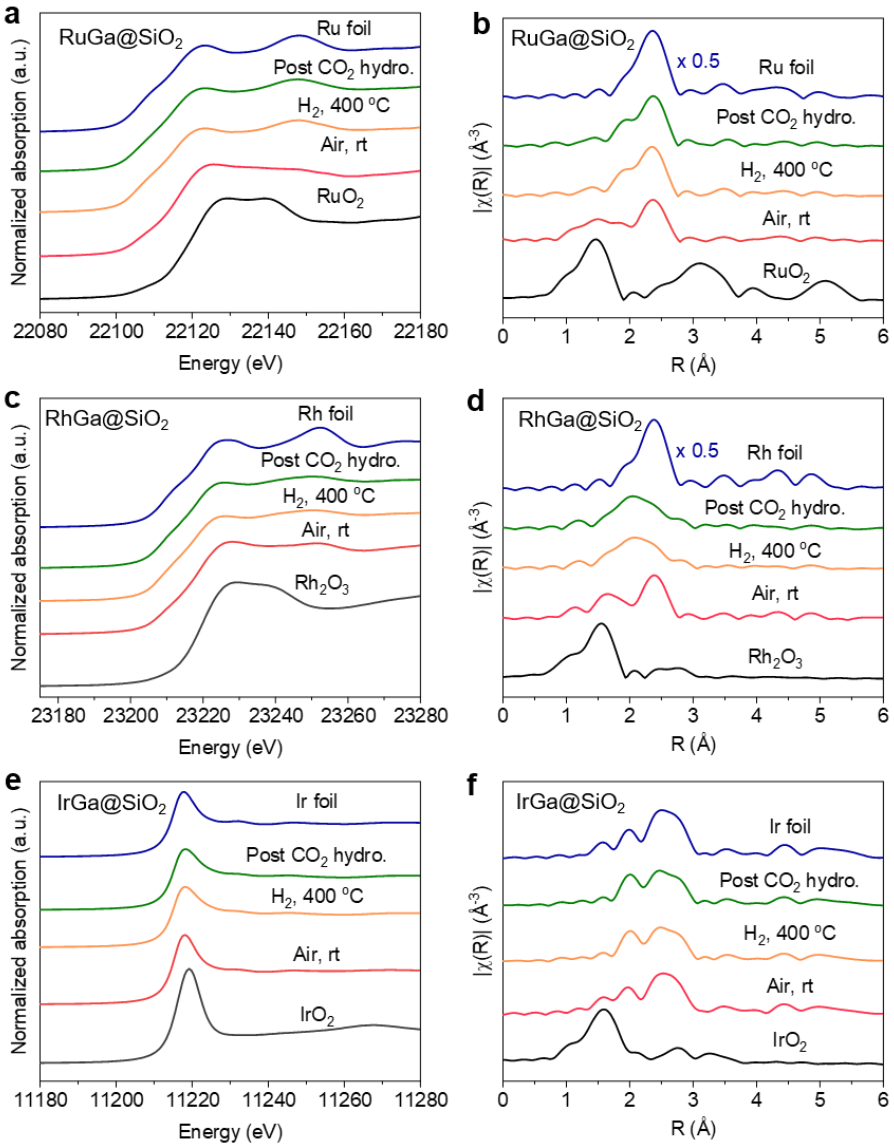

Fig. 3 | *In situ* XAS studies. XANES spectra and the k^2-weighted Fourier transforms of EXAFS spectra under different conditions for RhGa@SiO_2 at Rh K-edge (**a**) and (**b**); RuGa@SiO_2 at Ru K-edge (**c**) and (**d**); IrGa@SiO_2, and Ir L_3-edge (**e**) and (**f**) respectively.

In situ Diffuse Reflectance IR Fourier Transform Spectroscopy (DRIFTS) experiments were performed to monitor the observed intermediate species over Ga-promoted *M*Ga@SiO_2 catalysts (M = Ru, Os, Rh, and Ir) and monometallic *M*@SiO_2 during CO_2 hydrogenation at 20 bar. When the gas mixture of H_2/CO_2/Ar (3:1:1 – 20 bar) is introduced into the IR cell, a band at 2040-2070 cm^{-1} (adsorbed CO*), a band at 2170 cm^{-1} (gaseous CO) and a band at 3015 cm^{-1} (gaseous CH_4) can be observed over *M*Ga@SiO_2 catalysts (Supplementary Fig. 81) [27]. Besides the observed bands for gaseous CO and CH_4 and adsorbed CO*, two bands at around 2960 cm^{-1} and 2858 cm^{-1} are also detected. These two bands

can be assigned to adsorbed methoxy (CH_3O*) species, key intermediates for methanol formation[15,28]. Notably these methoxy species are not observed over monometallic Ru@SiO_2 and Rh@SiO_2 catalysts, while a rather high intensity band at 3015 cm^{-1} along with the weak rotational bands between 2600-3200 cm^{-1} are observed due to a high concentration of gaseous CH_4 (Supplementary Fig. 82)[29], consistent with the observed high methanation activity for CO_2 hydrogenation on Ru@SiO_2 and Rh@SiO_2. The same trend is also observed over Os-based and Ir-based catalysts. Note that slight methoxy bands after 30 min can also be detected over Ir@SiO_2, in agreement with the observation in CO_2 hydrogenation showing a non-negligible 7% intrinsic methanol selectivity (Fig. 2a, Table S2).

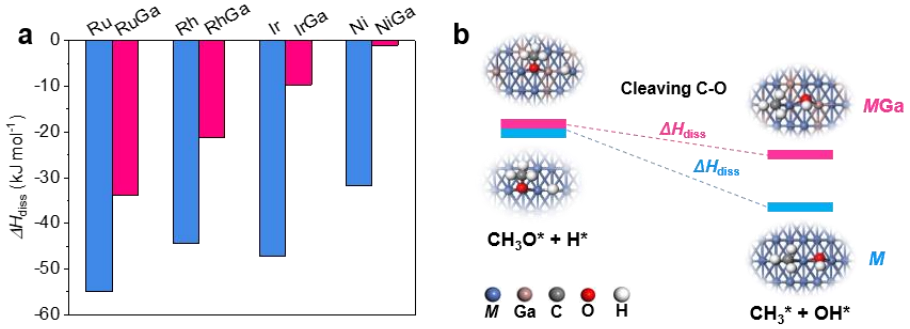

Fig. 4 | DFT calculation studies. (a) The dissociation enthalpies of C-O in methoxy on the representative {211} facet of different monometallic *M* and bimetallic *M*Ga (*M* = Ru, Rh, Ir and Ni) systems based on face-centered cubic (FCC) structure. (b) The scheme for cleaving the C-O bond of CH_3O* in the presence of H* on monometallic *M* and bimetallic *M*Ga.

To better understand the affinity of these metals towards alloying with Ga and how alloying prevents methanation, we also explore simple descriptors for alloying and for the capacity towards C-O bond cleavage on pure metal vs. alloyed surfaces using density functional theory (DFT) modelling. The affinity of the metals towards Ga is evaluated by calculating the alloy formation enthalpy ($\Delta H_{alloying}$) as a descriptor. We included Ni in this study because it is another well-known methanation catalyst, for which the presence of Ga has been shown to have similar promotional effects yielding methanol under CO_2 hydrogenation conditions[30]. Osmium has however been excluded due to the lack of experimental data (no XAS data, *vide supra*) and established work function dataset. For all these systems, a *M*/Ga (*M* = Ru, Rh, Ir and Ni) ratio of 3:1, close to the experimental ratio quantified by LCF analysis, is used for modelling the alloys. The alloy formation enthalpy ($\Delta H_{alloying}$) is evaluated by the energy difference between the metal in its most stable phase (FCC) and an alloy with a similar structure. In all four *M*Ga bimetallic systems, the values of $\Delta H_{alloying}$ are negative (Supplementary Fig. 83-87, Table S10),

indicating that Ga is readily incorporated into the *M* phase to form *M*Ga alloys for these metals, aligning with the aforementioned *in situ* XAS results.

With the *in-situ* DRIFTS experiments in hand, which indicate the presence of methoxy-species during the reaction over bimetallic MGa@SiO_2 catalysts while mostly methane is detected for M@SiO_2, we evaluate the propensity of C-O bond cleavage of adsorbed methoxy species in the presence of H adatoms on various metal surfaces using a representative {211} facet based on an FCC structure as a simple descriptor (Supplementary Fig. 88). Strongly negative dissociation enthalpies (ΔH_{diss}) are consistent with a favored C-O bond cleavage, while less negative values indicate a preferred methanol formation. As shown in Fig. 4, Supplementary Fig. 89-96, and Table S11 for all these four systems, the dissociation energy of C-O on monometallic *M* system is substantially more negative than that of the *M*Ga systems, suggesting that the cleavage of C-O yielding CH_3* species, which can be readily converted to CH_4, is more favorable on monometallic systems. In contrast, the presence of Ga in bimetallic *M*Ga alloys significantly weakens the capacity of C-O cleavage, thus stabilizing the methoxy species and promoting methanol formation. Combined with the *in situ* studies, we propose that the retained *M*Ga alloy during the CO_2 hydrogenation is key to suppressing the methanation reaction, while stabilizing the methoxy species and consequently promoting the formation of methanol.

In conclusion, this work shows that Ga displays a unique promotional effect, switching the catalytic properties of group 8 and 9 metals – Ru/Os and Rh/Ir – silica-supported nanoparticles from methanation to methanol synthesis under CO_2 hydrogenation conditions. The addition of Ga significantly decreases the rate of methanation in favor of the formation of oxygenates, in particular methanol and DME, hence the overall selectivity switch. *In situ* XAS studies indicate that the non-promoted monometallic *M* systems all remain metallic under CO_2 hydrogenation condition to show high activity for methanation reaction. However, the introduction of Ga generates *M*Ga alloys under a reductive H_2 atmosphere, and the *M*Ga alloy is stable under CO_2 hydrogenation conditions. *In situ* DRIFTS experiments and DFT calculations evidence that the presence of Ga in *M*Ga alloy is the key to stabilize methoxy species to promote methanol formation. Overall, Ga appears as a universal promoter for the reported well-known methanation catalysts converting them into methanol synthesis catalysts in CO_2 hydrogenation conditions. These observations provide insights to enable the rational design of catalysts and highlight how promoters can change the state and reactivity of transition-metal elements.

Supporting Information Additional Details for catalysts synthesis, crystal structures, routine characterization, DFT calculations and catalytic tests have been included in the Supporting Information.

Acknowledgements This publication was created as part of NCCR Catalysis (grant number 180544), a National Centre of Competence in Research funded by the Swiss National Science Foundation. C. C. and S. R. D. acknowledge the Swiss National Science Foundation (grants 200021_169134, and 200020B_192050), while C. E. acknowledges the Swiss National Science Foundation (grant 200020B_192050) and the Scholarship Fund of the Swiss Chemical Industry (SSCI). Prof. Dr. A. Comas-Vives is thanked for the scientific discussion on DFT studies, and Prof. Dr. M. P. Conley is thanked for developing the Ru precursor. The authors acknowledge Dr W. V. Beek and Dr D. Stoian at the Swiss Norwegian Beamlines (SNBL, ESRF) for the provision of beamtime and support with *in situ* XAS experiments *via* proposal A31-1-168 and A31-1-197. X. Zhou and K. Sakamoto are thanked for supporting experiment at the synchrotron. Furthermore, ScopeM is gratefully acknowledged for their support and assistance in this work through project No. 2460 and 2658. Crystal Data for Ru(*p*-Cymene)(OSi(O^{t}Bu)$_3$)$_2$, Os(*p*-Cymene)(OSi(O^{t}Bu)$_3$)$_2$ and Ir(COD)(DIA) can be obtained free of charge from Cambridge Crystallographic Data Centre (CCDC number: 2330054, 2329726 and 2329723)

Author Contributions W.Z., and C.C. conceived and designed the study. C.C. supervised the project. W.Z. and C.H. performed the catalyst preparation, catalytic reactions and most of characterizations. W.C. performed the theoretical calculation. E.B. performed the TEM experiments. Y.W. and C.W. performed the DRIFTS experiments. S.D. and C.E. assisted in in situ XAS and metal precursors synthesis. W.Z., C.H. and C.C. co-wrote the manuscript.

Author Information The authors declare no competing interest. Correspondence and requests for materials should be addressed to ccoperet@inorg.chem.ethz.ch.

References

1 Goeppert, A. *et al.* Recycling of carbon dioxide to methanol and derived products - closing the loop. *Chem. Soc. Rev.* **43**, 7995-8048, (2014).

2 Centi, G., Quadrelli, E. A. & Perathoner, S. Catalysis for CO_2 conversion: a key technology for rapid introduction of renewable energy in the value chain of chemical industries. *Energy Environ. Sci.* **6**, 1711-1731, (2013).

3 Olah, G. A., Prakash, G. K. S. & Goeppert, A. Anthropogenic chemical carbon cycle for a sustainable future. *J. Am. Chem. Soc.* **133**, 12881-12898, (2011).

4 Zhong, J. *et al.* State of the art and perspectives in heterogeneous catalysis of CO_2 hydrogenation to methanol. *Chem Soc Rev* **49**, 1385-1413, (2020).

5 Jiang, X. *et al.* Recent advances in carbon dioxide hydrogenation to methanol via heterogeneous catalysis. *Chem. Rev.*, (2020).

6 Amann P. *et al.* The state of zinc in methanol synthesis over a Zn/ZnO/Cu(211) model catalyst. *Science* **376**, 603-608, (2022).

7 Kattel S. *et al.* Active sites for CO_2 hydrogenation to methanol on Cu/ZnO catalysts. *Science* **355**, 1296-1299, (2017).

8 Li, M. M.-J. *et al.* Enhanced CO_2 hydrogenation to methanol over CuZn nanoalloy in Ga modified Cu/ZnO catalysts. *J. Catal.* **343**, 157-167, (2016).

9 Schumann, J. *et al.* Promoting strong metal support interaction: Doping ZnO for enhanced activity of Cu/ZnO:M (M = Al, Ga, Mg) catalysts. *ACS Catal.* **5**, 3260-3270, (2015).

10 Lam, E. *et al.* Enhanced CH_3OH selectivity in CO_2 hydrogenation using Cu-based catalysts generated via SOMC from Ga(III) single-sites. *Chem. Sci.* **11**, 7593-7598, (2020).

11 Sharafutdinov, I. *et al.* Intermetallic compounds of Ni and Ga as catalysts for the synthesis of methanol. *J. Catal.* **320**, 77-88, (2014).

12 Studt, F. *et al.* Discovery of a Ni-Ga catalyst for carbon dioxide reduction to methanol. *Nat. Chem.* **6**, 320-324, (2014).

13 García-Trenco, A. *et al.* Pd_2Ga-based colloids as highly active catalysts for the hydrogenation of CO_2 to methanol. *ACS Catal.* **7**, 1186-1196, (2017).

14 Liu, X. *et al.* Atomically thick oxide overcoating stimulates low-temperature reactive metal-support interactions for enhanced catalysis. *J. Am. Chem. Soc.* **145**, 6702-6709, (2023).

15 Docherty, S. R. *et al.* Silica-supported PdGa nanoparticles: metal synergy for highly active and selective CO_2 to CH_3OH hydrogenation. *JACS Au* **1**, 450-458, (2021).

16 Zhou, W. *et al.* Reactivity switch of platinum with gallium: from reverse water gas shift to methanol synthesis. *DOI: 10.26434/chemrxiv-2024-4j2gw*, (2024).

17 Vogt, C. *et al.* The renaissance of the sabatier reaction and its applications on earth and in space. *Nat. Catal.* **2**, 188-197, (2019).

18 Li, S. *et al.* Tuning the selectivity of catalytic carbon dioxide hydrogenation over iridium/cerium oxide catalysts with a strong metal–support interaction. *Angew. Chem. Int. Ed.* **56**, 10761-10765, (2017).

19 Molefe, T., Forbes, R. P. & Coville, N. J. Osmium@hollow carbon spheres as Fischer–Tropsch synthesis catalysts. *Catal. Lett.* **151**, 875-887, (2021).

20 Coperet, C. *et al.* Surface organometallic and coordination chemistry toward single-site heterogeneous catalysts: Strategies, methods, structures, and activities. *Chem. Rev.* **116**, 323-421, (2016).

21 Docherty, S. R. & Coperet, C. Deciphering metal-oxide and metal-metal interplay via surface organometallic chemistry: A case study with CO_2 hydrogenation to methanol. *J. Am. Chem. Soc.* **143**, 6767-6780, (2021).

22 Searles, K. *et al.* Silica-supported isolated gallium sites as highly active, selective and stable propane dehydrogenation catalysts. *Chem. Sci.* **8**, 2661-2666, (2017).

23 Heroguel, F. E. Controlled growth and inerfaces of supported metal nanoparticles from late transition metal siloxides. *ETH DISS. NO 21918*, (2014).

24 Zhou, W. *et al.* The promotional role of Mn in CO_2 hydrogenation over Rh-based catalysts from a surface organometallic chemistry approach. *Chem. Sci.* **14**, 5379-5385, (2023).

25 Elgayyar, T. *et al.* Contributions and limitations of IR spectroscopy of CO adsorption to the characterization of bimetallic and nanoalloy catalysts. *Catal. Today* **373**, 59-68, (2021).

26 Nakaya, Y. & Furukawa, S. Catalysis of alloys: Classification, principles, and design for a variety of materials and reactions. *Chem. Rev.* **123**, 5859-5947, (2023).

27 Mojet, B. L., Ebbesen, S. D. & Lefferts, L. Light at the interface: the potential of attenuated total reflection infrared spectroscopy for understanding heterogeneous catalysis in water. *Chem. Soc. Rev.* **39**, 4643-4655, (2010).

28 Collins, S. E. *et al.* Adsorption and decomposition of methanol on gallium oxide polymorphs. *J. Phys. Chem. C* **112**, 14988-15000, (2008).

29 Esler, M. B. *et al.* Precision trace gas analysis by FT-IR spectroscopy. 1. simultaneous analysis of CO_2, CH_4, N_2O, and CO in Air. *Anal. Chem.* **72**, 206-215, (2000).

30 Zimmerli N. K. *et al.* Structure and role of a Ga-promoter in Ni-based catalysts for the selective hydrogenation of CO_2 to Methanol. *JACS Au* **4**, 237-252, (2024).